Cancer Cell
Article

Integrative Genomic and Proteomic Analyses Identify Targets for *Lkb1*-Deficient Metastatic Lung Tumors

Julian Carretero,[1,2,13] Takeshi Shimamura,[1,3,13] Klarisa Rikova,[4] Autumn L. Jackson,[5] Matthew D. Wilkerson,[5] Christa L. Borgman,[1] Matthew S. Buttarazzi,[1,7] Benjamin A. Sanofsky,[1,7] Kate L. McNamara,[1,7] Kathleyn A. Brandstetter,[1,7] Zandra E. Walton,[1,7] Ting-Lei Gu,[4] Jeffrey C. Silva,[4] Katherine Crosby,[4] Geoffrey I. Shapiro,[1,3] Sauveur-Michel Maira,[8] Hongbin Ji,[9] Diego H. Castrillon,[10] Carla F. Kim,[11] Carlos García-Echeverría,[8] Nabeel Bardeesy,[12] Norman E. Sharpless,[5,6] Neil D. Hayes,[5] William Y. Kim,[5,6] Jeffrey A. Engelman,[12] and Kwok-Kin Wong[1,3,7,*]
[1]Department of Medical Oncology, Dana-Farber Cancer Institute, 44 Binney Street, Boston, MA 02115 USA
[2]Department of Physiology, Faculty of Medicine and Odontology, University of Valencia, Valencia 46010, Spain
[3]Department of Medicine, Brigham and Women's Hospital, Harvard Medical School, Boston, MA 02115, USA
[4]Cell Signaling Technology Inc., 3 Trask Lane, Danvers, MA 01923, USA
[5]Lineberger Comprehensive Cancer Center
[6]Department of Medicine and Genetics
The University of North Carolina at Chapel Hill, Chapel Hill, NC 27599, USA
[7]Ludwig Center at Dana-Farber/Harvard Cancer Center, 44 Binney Street, Boston, MA 02115, USA
[8]Novartis Institutes for Biomedical Research, Oncology Disease Area, CH4002 Basel, Switzerland
[9]Laboratory of Molecular Cell Biology, Institute of Biochemistry and Cell Biology, Shanghai Institutes for Biological Sciences, Chinese Academy of Sciences, 320 Yue Yang Road, Shanghai 200031, China
[10]Department of Pathology, University of Texas Southwestern Medical Center, Dallas, TX 75390, USA
[11]Children's Hospital Boston, 1 Blackfan Circle, 8-216, Boston, MA 02115, USA
[12]Massachusetts General Hospital Cancer Center, 185 Cambridge Street, Boston, MA 02114, USA
[13]These authors contributed equally to this work
*Correspondence: kwong1@partners.org
DOI 10.1016/j.ccr.2010.04.026

SUMMARY

In mice, *Lkb1* deletion and activation of $Kras^{G12D}$ results in lung tumors with a high penetrance of lymph node and distant metastases. We analyzed these primary and metastatic de novo lung cancers with integrated genomic and proteomic profiles, and have identified gene and phosphoprotein signatures associated with *Lkb1* loss and progression to invasive and metastatic lung tumors. These studies revealed that SRC is activated in *Lkb1*-deficient primary and metastatic lung tumors, and that the combined inhibition of SRC, PI3K, and MEK1/2 resulted in synergistic tumor regression. These studies demonstrate that integrated genomic and proteomic analyses can be used to identify signaling pathways that may be targeted for treatment.

INTRODUCTION

Lung cancer is the leading cause of cancer mortality worldwide. Genetic analyses and gene expression profiling of primary human lung tumors have identified several aberrant signaling pathways involved in the initiation of non-small cell lung cancer (NSCLC) (Bild et al., 2006). Although many of these pathways are also likely to be involved in NSCLC progression and metastases, it is clear that the metastatic phenotype requires additional pathway perturbations that regulate cell motility, cell adhesion, the epithelial to mesenchymal transition (EMT), and extracellular matrix remodeling (Nguyen and Massague, 2007). Because the development of metastases causes much of the morbidity and incurability of epithelial cancers, there is

Significance

Although large-scale genomic analyses of non-small cell lung cancers (NSCLCs) have yielded a better understanding of lung cancer genetic alterations, studies defining the pathways deregulated in tumor progression and metastases are limited. *LKB1* inactivation is found in up to 30% of human NSCLCs, and *Lkb1*-deficient lung tumors in mice have a high penetrance of lymph node and distant metastases. Our analyses of primary and metastatic *Lkb1*-deficient mouse lung tumors have shown that progression to metastatic lung cancer is associated with unique gene and phosphoprotein signatures. In this work, we employ these signatures to design an effective, rational therapeutic strategy to treat *Lkb1*-deficient lung cancers.

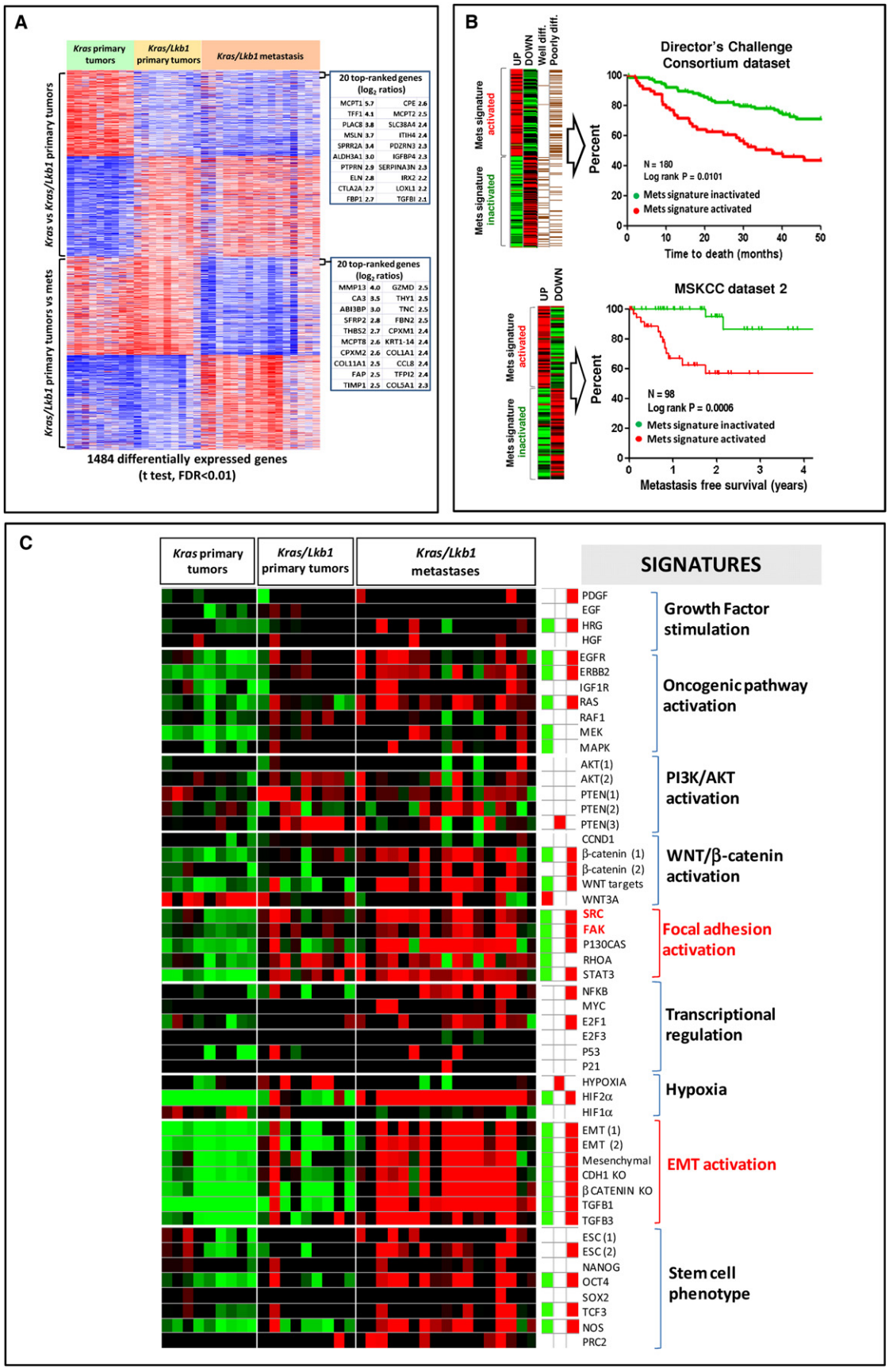
A
Kras primary tumors
Kras/Lkb1 primary tumors
Kras/Lkb1 metastasis
Kras vs Kras/Lkb1 primary tumors
Kras/Lkb1 primary tumors vs mets
20 top-ranked genes (log2 ratios)
MCPT1 5.7
CPE 2.6
TFF1 4.1
MCPT2 2.5
PLAC8 3.8
SLC38A4 2.4
MSLN 3.7
ITIH4 2.4
SPRR2A 3.4
PDZRN3 2.3
ALDH3A1 3.0
IGFBP4 2.3
PTPRN 2.9
SERPINA3N 2.3
ELN 2.8
IRX2 2.2
CTLA2A 2.7
LOXL1 2.2
FBP1 2.7
TGFBI 2.1
20 top-ranked genes (log2 ratios)
MMP13 4.0
GZMD 2.5
CA3 3.5
THY1 2.5
ABI3BP 3.0
TNC 2.5
SFRP2 2.8
FBN2 2.5
THBS2 2.7
CPXM1 2.4
MCPT8 2.6
KRT1-14 2.4
CPXM2 2.6
COL1A1 2.4
COL11A1 2.5
CCL8 2.4
FAP 2.5
TFPI2 2.4
TIMP1 2.5
COL5A1 2.3
1484 differentially expressed genes
(t test, FDR<0.01)
B
UP
DOWN
Well diff.
Poorly diff.
Mets signature activated
Mets signature inactivated
Director's Challenge Consortium dataset
Percent
N = 180
Log rank P = 0.0101
Mets signature inactivated
Mets signature activated
Time to death (months)
MSKCC dataset 2
N = 98
Log rank P = 0.0006
Metastasis free survival (years)
C
Kras primary tumors
Kras/Lkb1 primary tumors
Kras/Lkb1 metastases
SIGNATURES
PDGF
EGF
HRG
HGF
Growth Factor stimulation
EGFR
ERBB2
IGF1R
RAS
RAF1
MEK
MAPK
Oncogenic pathway activation
AKT(1)
AKT(2)
PTEN(1)
PTEN(2)
PTEN(3)
PI3K/AKT activation
CCND1
β-catenin (1)
β-catenin (2)
WNT targets
WNT3A
WNT/β-catenin activation
SRC
FAK
P130CAS
RHOA
STAT3
Focal adhesion activation
NFKB
MYC
E2F1
E2F3
P53
P21
Transcriptional regulation
HYPOXIA
HIF2α
HIF1α
Hypoxia
EMT (1)
EMT (2)
Mesenchymal
CDH1 KO
β CATENIN KO
TGFB1
TGFB3
EMT activation
ESC (1)
ESC (2)
NANOG
OCT4
SOX2
TCF3
NOS
PRC2
Stem cell phenotype

an urgent need to elucidate the events underlying this biological process.

The paucity of matched primary and metastatic human lung tumors has made it difficult to examine the genetic changes involved in the progression and metastasis of NSCLC. Studies using genetically engineered mice have demonstrated that the activation of certain combinations of oncogenes is sufficient for lung tumor initiation (Engelman et al., 2008; Jackson et al., 2001; Ji et al., 2006a, 2006b) and that additional genetic events are required for tumor progression (Iwanaga et al., 2008; Jackson et al., 2005) or metastases (Ji et al., 2007; Kim et al., 2009). We recently showed that the loss of the *Lkb1* tumor suppressor gene in *Kras*-driven lung tumors results in metastases to lymph node and distant sites in mice (Ji et al., 2007). Moreover, we and others have shown that *LKB1* is inactivated by point mutations or deletions in at least 15%–35% of NSCLC and concurrent *KRAS* and *LKB1* mutation is observed in 4%–10% of NSCLC (Carretero et al., 2004; Koivunen et al., 2008; Ji et al., 2007; Matsumoto et al., 2007; Sanchez-Cespedes et al., 2002).

In humans, germline mutation of *LKB1* results in the Peutz-Jeghers syndrome, a familial cancer syndrome characterized by intestinal hamartomas and an increased risk for epithelial cancers, including lung cancers (Hearle et al., 2006). The *LKB1* gene encodes a serine/threonine kinase that phosphorylates several substrates, many of which are also kinases (Alessi et al., 2006). However, identification of the pathways responsible for the prometastatic effects of *Lkb1* loss has yet to be made.

To identify altered signal transduction pathways involved in the progression and metastases of *Lkb1*-deficient lung tumors, we have performed an unbiased, integrated analysis of genomic and phosphoproteomic signatures of primary and metastatic mouse lung tumors.

RESULTS

Lkb1-Deficient Metastatic Lung Tumors Harbor Unique Gene Expression Changes

Lung-specific activation of mutant $Kras^{G12D}$ results in bronchoalveolar hyperplasia and low grade adenocarcinomas (Jackson et al., 2001). We recently observed that concomitant loss of the *Lkb1* tumor suppressor gene leads to a broadened histologic spectrum of lung tumors that have a high propensity for local invasion and metastases (Ji et al., 2007). To identify the gene expression changes associated with the invasive and metastatic progression of *Lkb1*-deficient mouse lung tumors, we compared RNA expression profiles from 9 *Kras* and 9 *Kras/Lkb1* primary tumors as well as 16 *Kras/Lkb1* metastases (lymph node and distant sites). Unsupervised hierarchical clustering of the samples revealed three distinct clusters corresponding to the following groups: (1) primary lung tumors with activated $Kras^{G12D}$, (2) primary lung tumors with activated $Kras^{G12D}$ and *Lkb1* loss, and (3) metastases from lung tumors with activated $Kras^{G12D}$ and *Lkb1* loss (see Figure S1A available online).

To better characterize the molecular alterations associated with *Lkb1* loss and metastasis, we derived expression signatures from our mouse lung tumors that reflected the gene expression changes induced by *Lkb1* loss in primary tumors (Lkb1) by comparing primary *Kras* tumors with primary *Kras/Lkb1* tumors and changes associated with metastases (Mets) by comparing *Kras/Lkb1* primary tumors to *Kras/Lkb1* metastases. We used a two-class unpaired differential expression analysis and a false-discovery rate (FDR) of < 0.01. The resulting "Lkb1" and "Mets" gene signatures contain 727 and 757 differentially expressed genes, respectively (Figure 1A). In aggregate, these results indicate that *Lkb1* loss induces significant transcriptional changes in primary cancers and that there are further gene expression alterations that characterize the progression to lymph node and distant metastasis.

A Cross-Species Comparison across Mouse and Human Data Sets Validates an Expression Signature of Metastases as Prognostic in Human NSCLC

We next sought to determine whether this Mets signature predicted clinical outcome in human lung cancer patients. Using the human orthologs of the murine genes in the Mets signature, we interrogated two publicly available gene expression data sets of primary NSCLCs, annotated for either overall survival and histologic grade (Director's Challenge Consortium data set, Shedden et al., 2008) or metastasis-free recurrence (MSKCC data set 2, Nguyen et al., 2009). The gene expression profiles of these human NSCLCs were queried for the presence or absence of our Mets expression signature as defined by coordinate upregulation and downregulation of overexpressed or underexpressed genes from the Mets signature.

Consistent with the notion that our Mets gene signature correlates with a proclivity toward metastasis, patients with tumors expressing the Mets signature had a significantly worse survival and increased occurrence of metastasis than did patients with tumors without Mets signature expression in these two data sets (Figure 1B). In contrast, the Lkb1 signature, generated by comparing *Kras* tumors to *Kras/Lkb1* primary tumors, had no prognostic value (data not shown). These data suggest that the same gene expression changes induced

Figure 1. A Gene Expression Signature of Metastasis Derived from a *Kras*-driven, *Lkb1*-Deficient Mouse Lung Cancer Model Predicts Survival in Human NSCLC

(A) Generation of an expression signature of metastasis. *Kras/Lkb1* primary tumors were compared with *Kras/Lkb1* metastases using two-class unpaired differential expression analysis and an FDR of < 0.01. A total of 757 unique transcripts were significantly differentially deregulated and used to define a metastatic gene signature (Mets).

(B) Kaplan-Meier analysis of the Director's Challenge Consortium data set (N = 180) and Memorial Sloan Kettering Cancer Center data set 2 (N = 98) of human lung tumors comparing the overall survival between tumors showing activation (red line) or inactivation (green line) of our mouse-derived Mets signature. The red line represents Mets signature activated. The green line represents Mets signature inactivated.

(C) Heat map of relative enrichment scores derived by gene set enrichment analysis. Tumors are represented in columns and genes signatures are represented in rows (red, significant enrichment of overexpressed genes; green, significant enrichment of under-expressed genes; black, not significant; $p < 0.05$). The right panel shows the aggregate enrichment scores for each of the three classes of tumors (*Kras*, *Kras/Lkb1* primary tumors and *Kras/Lkb1* metastases). See also Table S1 and Figure S1.

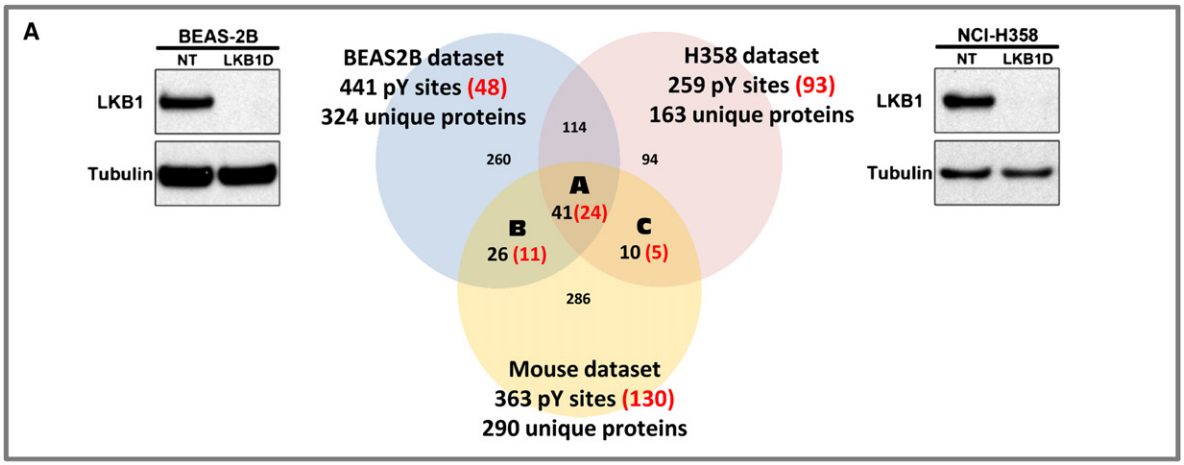

B

		Protein	Site	BEAS2B-LKB1D vs NT	H358-LKB1D vs NT	*Kras/Lkb1* primary vs *Kras*	*Kras/Lkb1* mets vs *Kras*	GEP DATA (vs *Kras*)	Upstream kinase	Description
CLUSTER A	Mouse ∩ BEAS2B ∩ H358	SRC	Y418	0.7	0.2	2.1	3.0		SRC, PDGFRA[1]	Protein kinase, Tyr (non-receptor)
		FAK	Y576	0.8	1.2	2.6	1.4		SRC, FAK, INSR, RET[1]	Protein kinase, Tyr (non-receptor)
		GPRC5A	Y347,Y350	0.9	1.8	4.1	1.5		IGF1R, INSR[2]	Receptor, channel, transporter or cell surface protei
		F11R	Y280	2.1	1.1	2.7	0.9		IGF1R, ABL1, INSR[2]	Adhesion or extracellular matrix protein
		DYRK2	Y264,Y382	1.5	0.6	1.5	0.5		EPHA3, CSF1R, KIT, ITK, BTK, MAP2K3[2]	Protein kinase, dual-specificity
		CDCP1	Y707	1.8	-0.4	3.3	2.0		SRC[1]	Receptor, channel, transporter or cell surface protei
		HCK	Y396,Y410	2.1	0.8	0.1	1.3		HCK[1]	Protein kinase, Tyr (non-receptor)
		ANXA2	Y23	-0.3	-0.2	3.2	1.3		SRC[1]	Calcium-binding protein
		ANXA2	Y29	-0.6	1.0	3.1	2.6		SRC[1]	Calcium-binding protein
		ABL1	Y393,Y412,Y439	0.1	0.3	-0.3	2.4		SRC, ABL1[1]	Protein kinase, Tyr (non-receptor)
		STAT3	Y704	0.1	-0.2	2.3	-0.2		JAK2[1]	Transcriptional regulator
		STAT3	Y705	-2.0	0.0	3.3	0.6		SRC, JAK2, ALK, JAK1, RET, FGFR3, FGFR4, HCK[1]	Transcriptional regulator
		PXN	Y118	-0.7	0.9	1.8	0.6		SRC, FAK, ABL1, EPHB1, PTK6[1]	Adaptor/scaffold
		PTPRA	Y798,Y789	-1.1	0.4	3.2	1.6		SRC[1]	Phosphatase
		PTPN11	Y62	-0.6	0.3	2.3	0.2		IGF1R, INSR[2]	Phosphatase
		HIPK1	Y352,Y361	-0.1	0.7	0.8	-1.2		IGF1R, INSR[2]	Protein kinase, Ser/Thr (non-receptor)
		DYRK1A	Y321,Y273	0.1	0.6	0.3	-1.3			Protein kinase, dual-specificity
		MAPK13	Y182	2.1	-0.1	0.0	-1.9			Protein kinase, Ser/Thr (non-receptor)
		PDHA1	Y299,Y301	0.8	0.2	1.6	-0.9		PRKCA[1]	Enzyme, glycolysis
		GRLF1	Y1105	-0.4	0.6	1.7	-0.5		SRC[1]	G protein or regulator
		CDC2	Y15	-3.1	0.7	0.6	-0.2		WEE1, PKMYT1, LYN[2]	Protein kinase, Ser/Thr (non-receptor)
		MAPK1	Y186	-2.7	0.9	0.7	-1.2		JAK2, MAP2K1, MAP3K8, MAP2K1, MAPK1, RET[1]	Protein kinase, Ser/Thr (non-receptor)
		MAPK3	Y204	-1.2	0.8	0.7	-2.3		JAK2, MAP2K1, MAP2K2, MAP3K8[1]	Protein kinase, Ser/Thr (non-receptor)
		MAPK14	Y181,Y182	0.2	0.3	-0.6	-1.2		MAP2K3, MAP2K6, RET[1]	Protein kinase, Ser/Thr (non-receptor)
CLUSTER B	Mouse ∩ BEAS2B	MYH9	Y1408	0.6		2.0	2.1			Motor or contractile protein
		TNS1	Y1480	0.0		2.6	4.1			Adaptor/scaffold
		VCL	Y692	0.0		1.5	1.8			Adhesion or extracellular matrix protein
		STAT5A	Y694	0.0		2.1	1.7		SRC, JAK2, LYN, BTK[1]	Transcriptional regulator
		SGK269	Y632	-0.3		-2.2	1.2			Protein kinase, Ser/Thr (non-receptor)
		FLJ32810	Y789	-0.7		4.6	1.9			G protein or regulator
		AXL	Y696	1.3		0.7	0.0		AXL[1]	Protein kinase, Tyr (receptor)
		PTRF	Y310	1.3		-0.8	-1.5			Transcriptional regulator
		MYH10	Y1415	-0.2		0.9	-1.1			Motor or contractile protein
		PIK3R1	Y467	-1.7		-1.3	-0.6			Kinase (non-protein)
		PIK3R1	Y452	-1.7		-1.8	-1.2			Kinase (non-protein)
CLUSTER C	Mouse ∩ H358	EPS8	Y525		1.8	4.1	1.8		EGFR[1]	EGFR signaling via small GTPases
		ACTA1	Y53,Y55,Y54		1.1	2.6	1.2		IGF1R, INSR[2]	Cytoskeletal protein
		PRKCD	Y313		1.3	2.2	1.1		SRC, LCK, EGFR, PDGFRA, PTP1B, ABL[2]	Protein kinase, Ser/Thr (non-receptor)
		SHIP2	Y986		1.9	1.4	0.3		SRC[1]	Phosphatase
		PRPF4B	Y849		-0.7	-2.1	-5.2			Protein kinase, Ser/Thr, pre-mRNA processing

during progression of *Lkb1* deficient tumors to metastases in this murine model faithfully recapitulate those associated with the development of advanced incurable disease in human primary NSCLC and might be useful to prognosticate patients with early stage lung cancer. The disparity in the ability of the Lkb1 signature and the Mets signature in predicting survival suggest that either there is a subset of cells in the primary tumor that is destined for metastases that cannot be discerned from expression analyses of the whole tumor or that additional expression changes developed at the site of metastases from cancer-stromal cell interactions. Lastly, and as shown on Figure S1B, the repressed component of the Mets signature showed a strong and significant correlation with the human samples that are mutant for both *KRAS* and *LKB1* in the University of North Carolina data set (Ji et al., 2007).

Lkb1-Deficient Metastases have Upregulation of EMT-Associated Gene Signatures

Activation of oncogenic signaling pathways has been shown to induce broad gene expression changes that can be used to generate gene expression or metagene signatures (Nevins and Potti, 2007). In order to better understand the biological basis for tumor metastasis in this model, we compared genes that were upregulated in the metastatic progression of these mouse lung tumors to known lists of transcripts associated with specific alteration in known pathways. Using gene set enrichment analyses, we identified gene signatures that were significantly enriched in our *Kras/Lkb1* metastases relative to our primary *Kras* and *Kras/Lkb1* lung tumors (Segal et al., 2004). Specifically, a collection of curated gene sets (Table S1) provided by the Molecular Signatures Database (MsigDB, broad.mit.edu/gsea/msigdb) and those collected from the literature (Ben-Porath et al., 2008; Bild et al., 2006; Cole et al., 2008; Onder et al., 2008) were used to interrogate our gene expression data set with the Genomica analysis tool (genomica.weizmann.ac.il).

A total of 32 of the 51 curated, cancer-related, gene sets appeared to be significantly enriched and highly expressed ($p < 0.05$, FDR < 0.05) in our data set of *Kras/Lkb1* metastases relative to *Kras* and *Kras/Lkb1* primary lung tumors (Figure 1C). This included a number of gene signatures implicated in the metastatic process such as focal adhesion alterations, EMT, increased TGF-β and β-catenin signaling, as well as embryonic stem (ES) cell expression signature and transcription factors implicated in ES cell phenotype such as TCF3 and OCT4 (Ben-Porath et al., 2008; Bild et al., 2006; Cole et al., 2008; Onder et al., 2008). A number of these findings were validated. For example, the canonical EMT markers (Kalluri and Weinberg, 2009), Vimentin, Snail, Twist1, N-cadherin, Acta2, and fibronectin seen in this signature were validated by real-time polymerase chain reaction (RT-PCR) (Figure S1C). Multiplex bead assay confirmed the elevated TGF-β levels in lysates from *Kras/Lkb1* metastases (Figure S1D). Furthermore, immunostaining demonstrated the presence of canonical EMT markers such as vimentin and fibronectin in both *Kras/Lkb1* primary and metastatic tumors (Figure S1E). Although components of these oncogenic signatures were observed in *Lkb1*-deficient primary tumors, their levels appeared to be higher in *Lkb1*-deficient metastases (Figure 1C and Figures S1C–S1E). These results suggest that additional molecular events cooperate with *Lkb1* loss to maximally activate these pathways during metastatic progression.

Phosphoscan of *LKB1*-Deficient Cells Identifies Activation of SRC Family Kinases

To complement our transcriptional analysis, we assessed how loss of *Lkb1* impacted tyrosine kinase signaling cascades. We hypothesized that if *Lkb1* loss resulted in significant activation of specific tyrosine kinases, then we should detect increased phosphorylation of their respective substrates. To complement the analysis of murine tumors, we generated paired *LKB1* and control knockdown cells in the BEAS-2B human bronchial epithelial cell line (Reddel et al., 1988), which is immortalized with SV40 Large T antigen, (BEAS-2B-LKB1D and BEAS-2B-NT, respectively) and in the *KRAS* mutant, *LKB1* wild-type NSCLC cell line H358 (H358-LKB1D and H358NT), which has been previously shown not to express markers of EMT (Thomson et al., 2008) (Figure 2A). These paired human cell lines, along with our mouse lung primary and metastatic tumors, were used for generating phosphotyrosine signatures with previously described methods (Rikova et al., 2007). Specifically, whole cell extracts from cell lines or pooled tissue lysates (two pools with three tumor samples each from *Kras, Kras/Lkb1* primary tumors, and *Kras/Lkb1* metastases) were immunoprecipitated with a phosphotyrosine specific antibody, and the immunoprecipitates were subjected to mass spectrometry (MS) analysis to identify and quantify phosphopeptides.

We identified 441, 259, and 363 phosphotyrosine sites in BEAS-2B, H358 and mouse lung tumors, respectively, that were enriched in the absence of LKB1 (Figure 2A). Forty-one of these LKB1-affected tyrosine phosphorylated peptides were noted to overlap across all three data sets (Figure 2A, cluster A), whereas an additional 26 peptides and 10 peptides were noted to overlap between the BEAS-2B / mouse tumor and H358 / mouse tumor data sets, respectively (Figure 2A, clusters B and C). An examination of the putative upstream kinases

Figure 2. Phosphoprotein Profiling of Human Cell Lines and Murine Tumors

(A) Venn diagram of phosphotyrosine sites identified in *Kras/Lkb1* primary versus metastatic murine tumors and isogenic paired cell lines (NCI-H358 and BEAS-2B) expressing shRNA to LKB1 (LKB1D) or a nontargeting shRNA (NT). Western blots show the effectiveness of LKB1 knockdown (LKB1D) in NCI-H358 and BEAS-2B cells. Red numbers in brackets show differentially increased or decreased phosphotyrosine sites in each comparison.

(B) Table of coordinately regulated, LKB1-dependent phosphotyrosine sites. Details of the LKB1-dependent phosphotyrosine sites found to be coordinately regulated across data sets are listed and include the phosphorylated protein, the tyrosine site, heatmaps of log2 ratios of indicated comparisons (red, positive log2 ratios; blue, negative log2 ratios), as well as the putative upstream kinase. The GEP (gene expression profiling) data column indicates the level of expression of the genes encoding these proteins between *Kras/Lkb1* (primary or mets) versus *Kras* murine tumors comparisons (red dots = significantly overexpressed, green dots = significantly underexpressed, and orange dots = no significant change). Subscript 1 indicates upstream kinases obtained from PhosphoELM, HPRD and Swissprot databases. Superscript 2 indicates upstream kinases obtained from NetworKIN database (see also Figure S2).

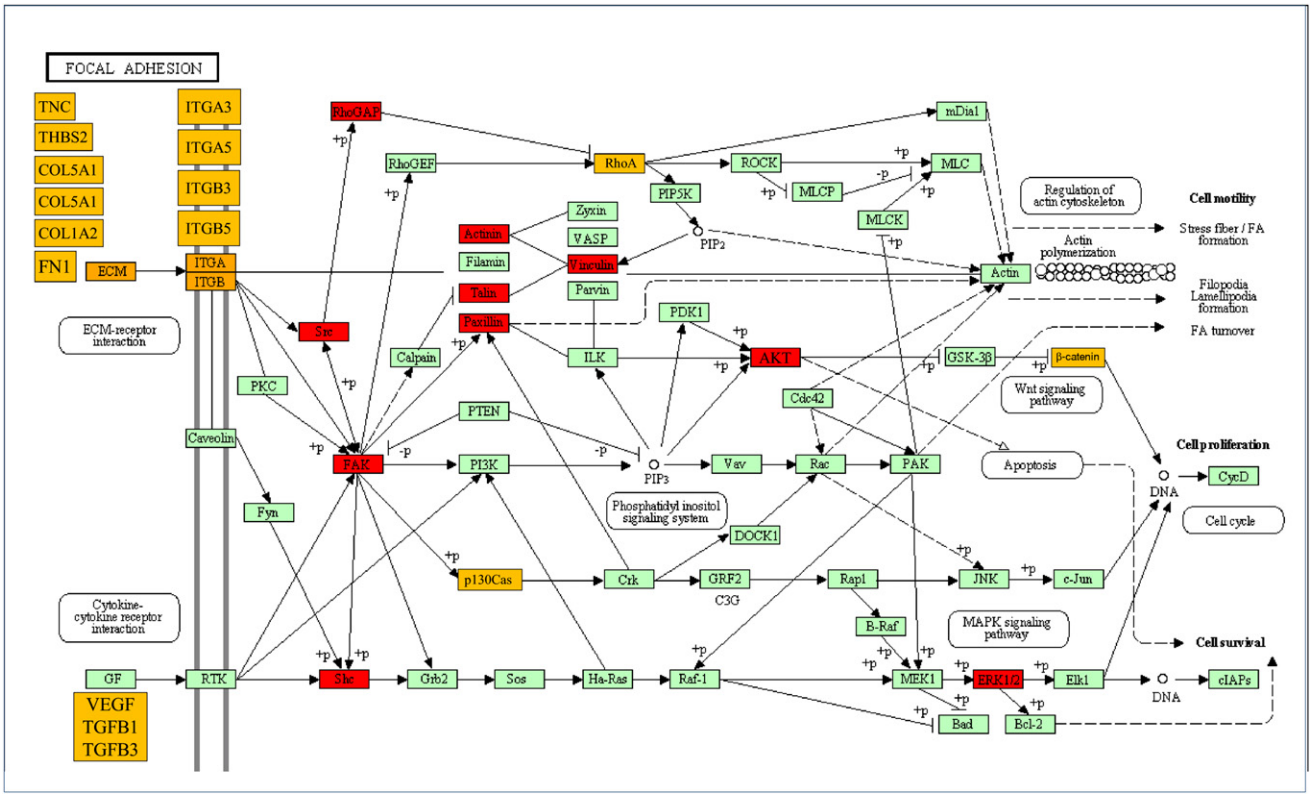

Figure 3. Focal Adhesion Is Impaired in *Kras/Lkb1* Tumors and Metastases

Most relevant findings from our genomic and proteomic analysis were depicted on the focal adhesion KEGG pathway. Proteins labeled in red were hyperphosphorylated in the Phosphoscan analysis comparing *Kras/Lkb1* primary tumors and metastases within the Phosphoscan analysis comparing *Kras/Lkb1* primary tumors and metastases with *Kras* alone tumors (Figure 2B). Proteins labeled in orange were found overexpressed (or their signatures were enriched) in the gene expression profiling comparing *Kras/Lkb1* primary tumors and metastases with *Kras* alone tumors (Figures 1A and 1C).

known to phosphorylate these tyrosine residues suggested that a number of kinases were activated in association with LKB1 deficiency. These analyses pointed to a particularly central role for SRC activation that was not only highly phosphorylated, but that is also predicted to be an upstream kinase for 13 sites of 40 differentially phosphorylated proteins among our data sets (Figure 2B). Moreover, *Kras/Lkb1* primary tumors and metastases showed a significant hyperphosphorylation of a Src substrates signature, as assessed by Gene Set Enrichment Analysis (GSEA) (Figure S2A).

The Nonreceptor Tyrosine Kinases, SRC and Focal Adhesion Kinase, Are Activated by *LKB1* Loss

We speculated that integration of the gene expression and phosphoproteomics data sets would be a powerful approach to identify functionally significant molecular alterations in *Lkb1*-deficient lung cancers. We noted that gene signatures of focal adhesion activation were highly enriched in metastases from *Kras/Lkb1* lung tumors (Figure 1C). Focal adhesions are dynamic subcellular structures known to mediate cell attachment to the extracellular matrix and are composed of over 50 proteins including focal adhesion kinase (FAK or PTK2), Paxillin, and SRC (Burridge et al., 1997; Playford and Schaller, 2004; Yeatman, 2004). As noted above, SRC activation was the most prominent signature emerging from our phosphoproteomic analysis and there was also strong evidence for FAK activation. To better integrate our data examining the impact of LKB1 loss on the focal adhesion pathway, components of the pathway upregulated at the gene expression or tyrosine phosphorylation level were colored yellow and red, respectively, and visualized on a KEGG pathway map (Figure 3). The results appear to show convergence on the activation of SRC, FAK, and their downstream pathways by *Lkb1* loss and implicate alterations in the expression and activity of focal adhesion regulators in the pathogenesis of *Lkb1*-deficient lung cancers.

SRC and FAK activation results in focal adhesion disassembly and turnover, through downregulation of RhoA, resulting in increased cellular motility (Arthur et al., 2000; Yeatman, 2004). Given the key role of cellular motility and migration in the process of metastasis, we next determined whether LKB1 regulates these key components of focal adhesion dynamics. To this end, whole cell extracts of the H358 cells expressing control shRNA (NT) or four different shRNA sequences targeting LKB1 (A, B, C, and D) were immunoblotted using antibodies against the activating tyrosine phosphorylation sites in SRC, and FAK (Y416 and Y576/577, respectively). As shown in Figure 4A, LKB1 knockdown led to activation of the focal adhesion complex, specifically SRC and FAK. Moreover, consistent with LKB1's established role as a regulator of the AMPK/TSC/mTORC1 axis (Carretero et al., 2007; Shaw et al., 2004), H358 *LKB1*-deficient

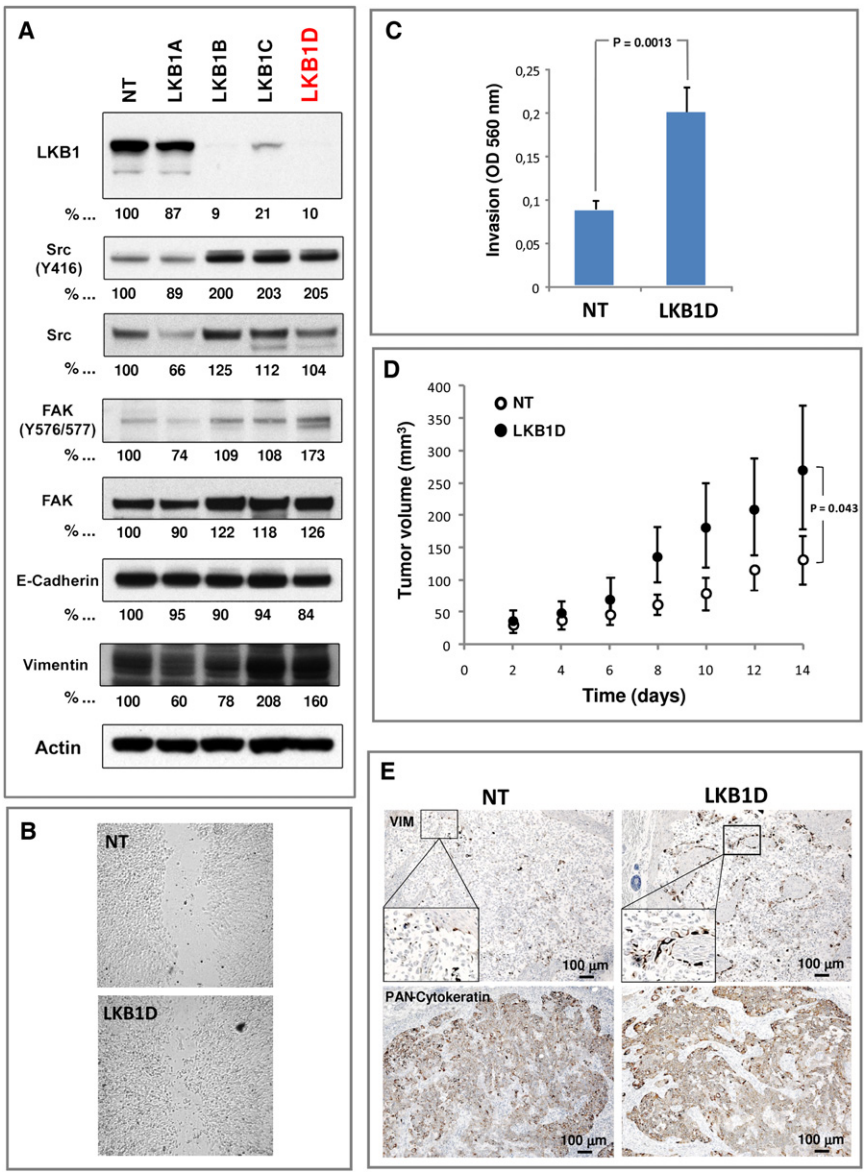

Figure 4. LKB1 Knockdown Activates EMT Markers, Mediators of Focal Adhesion Dynamics, and Enhances Cell Motility

(A) Western blot analysis of NCI-H358 cells (*LKB1* wild-type, *KRAS* G12C mutant) infected with lentiviruses encoding four different sequences of shRNAs (LKB1A– LKB1D) targeting LKB1 or nontargeting shRNA (NT). Whole cell lysates were imunoblotted with antibodies specific to LKB1 or tyrosine-specific antibodies against SRC (Total and Y416), FAK (Total and Y576), paxillin (Total and Y118), E-Cadherin, and vimentin. α/β-Actin (Actin) serves as a loading control.

(B) Representative photographs of scratched areas of confluent monolayers of NCIH358 cells expressing a shRNA to LKB1 (LKB1D) or a nontargeting shRNA (NT) 12 hr after wounding with a pipet tip.

(C) NCI-H358 cells expressing shRNA to LKB1 (LKB1D) or nontargeting shRNA (NT) were subjected to invasion assay in Boyden chambers coated with matrigel for 48 hr using 10% FBS as chemoattractant. Data is graphed as mean of three replicates and standard deviation (± SD).

(D) Mean tumor volume measurements of NCI-H358 xenografts. The human lung cancer cells, NCI-H358, expressing shRNA to LKB1 (LKB1D) or a nontargeting shRNA (NT) were grown subcutaneously in athymic nude mice. After 14 days the tumors were measured and the tumor volume calculated (error bars represent 1 SD; n = 5, p = 0.043).

(E) Immunohistochemical staining of human vimentin and human cytokeratins in NCIH358 NT and LKB1D xenografts. See also Figure S3.

cells showed an increase of AMPK (T172) and decrease of ACC (S79) phosphorylation, as well as an increase of S6 (S240/S244) phosphorylation (Figure S3A).

Because Phosphoscan and western blot analyses detect a phosphorylation site (Y416) that is common to all SRC family kinases (SFKs) including SRC, FYN, LYN, LCK, HCK FGR, and YES, we interrogated the phosphorylation status of SFKs affected by LKB1 loss in NCI-H358 and A549 cell lines using a Luminex bead assay. As shown in Figures S3B and S3C, H358 cells preferentially activate SRC and LYN, whereas A549 activates only SRC. In both cases, LKB1 loss promoted activation of SFKs. In addition, analyses of the protein lysates from H358-LKB1D and H358-NT cells with a protein array with site-specific phosphoantibodies further validated SRC, FAK, and other targets obtained by MS analyses of *Kras/Lkb1* murine model (Figure S3D).

These changes in SRC and FAK suggest impaired adhesion and increased cellular motility (Yeatman, 2004). To assess whether loss of *LKB1* affects the motility of these NSCLC cells, we performed a scratch assay. H358 cells with LKB1 knockdown (LKB1D) migrated more rapidly into the scratched space than the control cells (NT), whereas proliferation and viability of the two cells lines were identical in vitro (Figure 4B and Figure S3E). LKB1 loss also increased in vitro invasion of H358 cells, as assessed by Boyden chamber assay (Figure 4C). Therefore, loss of LKB1 appears to increase the kinase activity of several key proteins involved in focal adhesion dynamics and promote cell motility and invasion.

We also determined the consequences of LKB1 loss in NSCLC cells in vivo. To this end, we grew H358-LKB1D and H358-NT cells as subcutaneous xenograft tumors in nude mice and measured mean tumor volume 2 weeks after implantation. Tumors derived from H358 LKB1-deficient cells were significantly larger than those expressing a nonspecific shRNA, suggesting that loss of LKB1 promotes primary tumor growth in addition to metastasis (Figure 4D). Immunohistochemical (IHC) staining with antibodies that specifically recognize human (but not mouse) antigens showed increased levels of vimentin in the

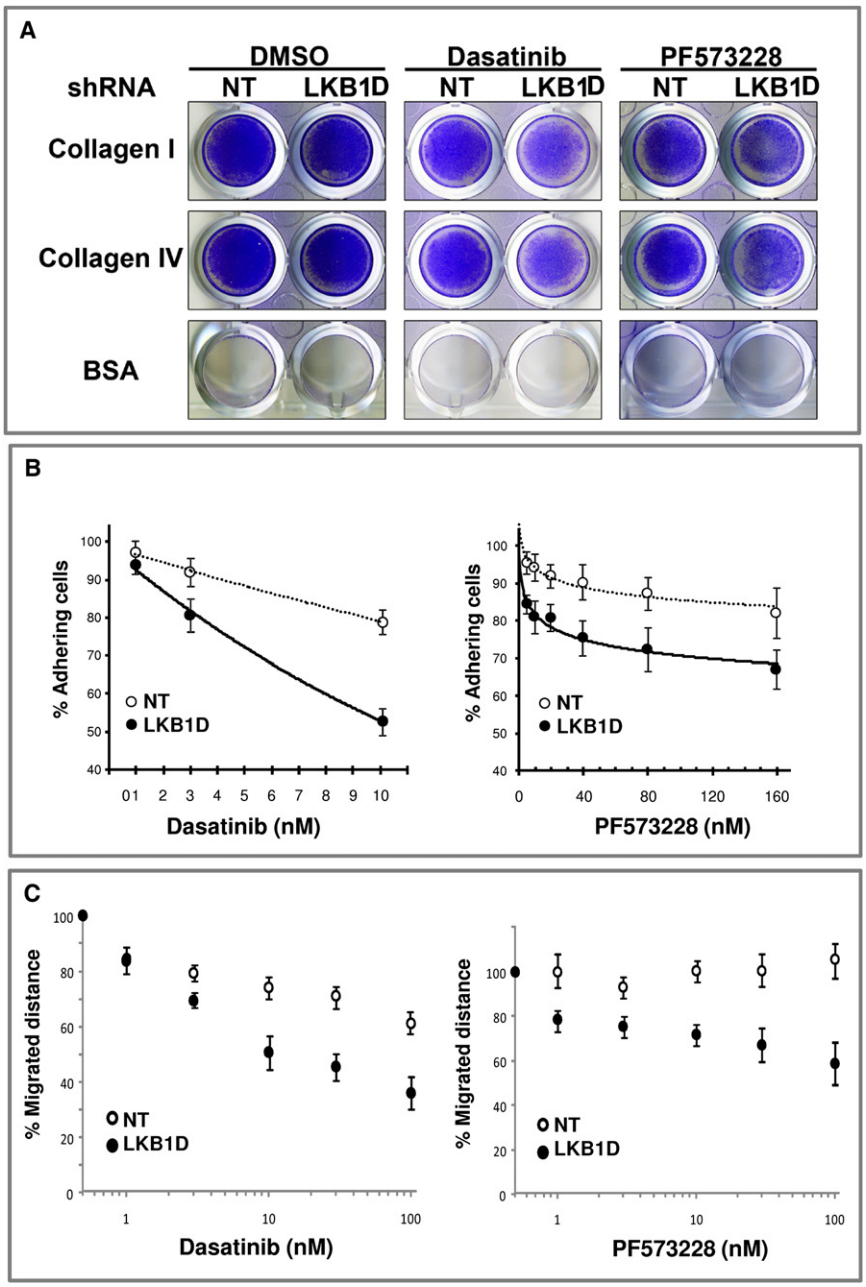

Figure 5. LKB1 Knockdown Cooperates with FAK and SRC Inhibition to Prevent Adhesion to Collagen and Migration in NCI-H358 Cells

(A) Exponentially growing NCI-H358 cells expressing shRNA to LKB1 or a nonspecific shRNA (NT) were seeded at 5 × 10^5 cells in wells coated with collagen I, collagen IV, or bovine serum albumin and allowed to adhere to the matrices in the presence of dimethyl sulfoxide (DMSO, control), 10 nM Dasatinib (SRC inhibitor) or 100 nM PF 573228 (FAK inhibitor). After 90 min, loose cells were washed off and adherent cells were fixed and stained.

(B) NCI-H358 cells expressing shRNA to LKB1 (LKB1D) or a nonspecific shRNA (NT) were seeded at 1 × 10^5 cells/well onto collagen I-coated 96-well plates containing DMSO or increasing concentrations of Dasatinib or PF573228, and incubated for 90 min. Data points represent the average of normalized values expressed as percentage of adhesion compared with DMSO-treated cells, from two independent experiments performed in triplicate; error bars represent SD.

(C) NCI-H358 cells expressing shRNA to LKB1 (LKB1D) or a nonspecific shRNA (NT) were seeded at 1 × 10^5 cells/well onto 24 wells, and cells were allowed to grow until forming confluent monolayers. The monolayer was scratched with a pipet tip to form a wound and the cells were grown in media containing DMSO or increasing concentrations of Dasatinib or PF573228. Twelve hours after wounding of the confluent monolayers, the wound closure was measured and expressed as percentage closure of the original wound. Data are graphed as mean of three replicates ± SD.

H358-LKB1D xenografts than in the H358-NT tumors (Figure 4E), in agreement with the previous results suggesting that loss of *LKB1* promotes EMT (Figure 4A and Figure S1E). Elevated vimentin staining was particularly prominent at the edge of tumors suggesting that the EMT in the *LKB1*-deficient tumor cells may have also involved signals from the adjacent stromal cells (Figure 4E). In agreement to these observations, H358 cells without LKB1 (LKB1D) released significantly more TGF-β1/2 than H358 control (NT) cells and nuclear β-catenin accumulation was more prevalent in LKB1D than in NT cells (Figures S3F and S3G). These observations support the notion that LKB1 loss plays an important role in EMT.

LKB1 Loss Heightens Dependence on SRC and FAK Signaling for Cell Adhesion and Migration

Our integrated gene expression and Phosphoscan results suggest that LKB1 loss might promote metastasis through activation of SRC and FAK signaling. Metastasis is a multistep process involving cell interactions with extracellular matrix (ECM) components, increased cell migration and tumor invasion (Mitra and Schlaepfer, 2006). These individual processes can both modulate and be modulated by SRC and FAK activity (Huveneers and Danen, 2009; Shibue and Weinberg, 2009). We hypothesized that SRC/FAK activation induced by LKB1 loss resulted in an increased dependence upon these signaling pathways for cell adhesion to ECM. To test this hypothesis, we plated 5 × 10^5 cells with or without LKB1 knockdown on tissue culture wells coated with collagen I, collagen IV, fibronectin, laminin I, fibrinogen, or BSA in the presence of the SRC-family kinase inhibitor Dasatinib or the FAK inhibitor PF573228 (Johnson et al., 2005; Slack-Davis et al., 2007). Among the ECM components tested, only collagen I or IV could promote the adherence of H358 cells (Figure 5A and data not shown). Knockdown of LKB1 in H358 cells did not have

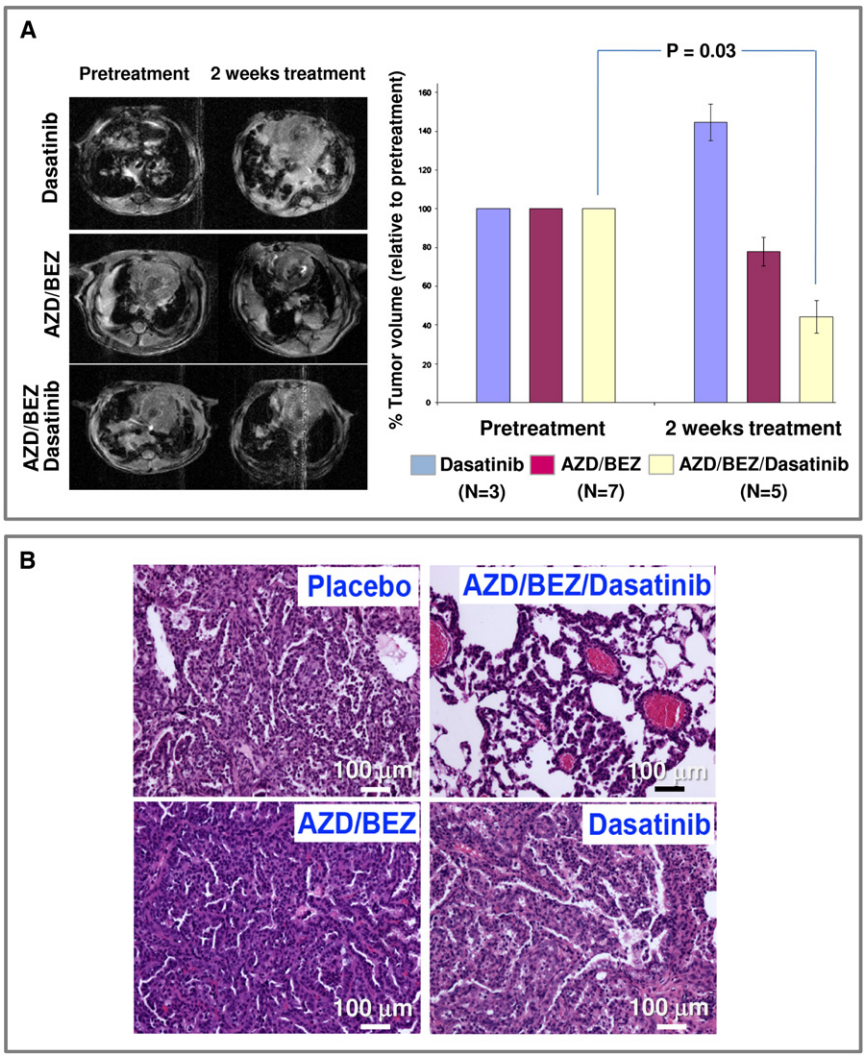

Figure 6. Combination Therapy with PI3K, MEK, and SRC Inhibitors Results in Synergistic In Vivo Response of *Lkb1*-Deficient Murine Lung Tumors

(A) Representative MRI images before and after treatment for each group. Mice in each group were MRI imaged then treated daily for 2 weeks with 45 mg/kg BEZ235, 25 mg/kg AZD6244, and 15 mg/kg Dasatinib, and imaged again. Tumor volumes were normalized to pretreatment tumor volumes. The average tumor volumes of three to seven mice in each treatment group are shown. Error bars represent 1 SD ($p < 0.05$ BEZ/AZD/Dasatinib treated versus pretreatment).

(B) H&E staining. H&E sections of representative *Kras/Lkb1* tumors from animals treated with the indicated drugs. See also Tables S2 and S3.

an appreciable effect on the baseline adhesion of H358 cells to either collagen I or IV. However, treatment of H358 cells with Dasatinib or PF573228 resulted in a dose-dependent decrease in cell adhesion that was more prominent in H358 cells with LKB1 knockdown (Figure 5B). Similar results were obtained when H358 cells with or without LKB1 expression were examined for the effects of Dasatinib and PF573228 on cell migration (Figure 5C). These observations support the notion that the activation of SRC and FAK due to LKB1 loss promotes dependence upon these signaling pathways for cell migration and adhesion to extracellular matrix components as well as migration.

Combined Inhibition of PI3K-mTOR, MEK, and SRC Family Kinases Results in Synergistic In Vivo Tumor Response in *LKB1*-Defective Lung Tumors

We had previously observed that dual inhibition of PI3K-mTOR and MEK with BEZ235 (a PI3K-mTOR inhibitor) and AZD2644 (a MEK1/2 inhibitor) resulted in an 80% reduction of tumor volume of Kras-dependent murine lung tumor model (Engelman et al., 2008). Surprisingly, treatment of *Kras/Lkb1* mice with the same combination showed that these lung tumors were largely unresponsive (Figure 6A). Because our integrated gene expression and phosphotyrosine profiling as well as in vitro cell culture studies demonstrated that SRC is activated by *LKB1* loss (Figures 1C and 2B, and Figures S2 and S3A–S3C), we hypothesized that inhibition of SRC by Dasatinib might restore sensitivity of *Kras/Lkb1* lung tumors to PI3K and MEK inhibition. To examine the therapeutic impact of SRC inhibition in *Kras/Lkb1* lung cancers, we treated established *Kras/Lkb1* lung cancers with Dasatinib alone, the combination of BEZ235 and AZD2644 (AZD/BEZ), or the combination of all three agents (Dasatinib/AZD/BEZ). Although *Kras/Lkb1* lung tumors did not respond to Dasatinib or BEZ/AZD, the triple combination Dasatinib/BEZ/AZD resulted in significant tumor regression as detected by serial magnetic resonance imaging (MRI) (Figure 6A) and histology (Figure 6B). These in vivo data suggest that *Lkb1* loss results in reduced sensitivity to the combined inhibition of PI3K and MEK, at least in part, through activation of SRC. Moreover, although Dasatinib alone in *Kras/Lkb1* lung cancer model did not provide overall survival benefit over vehicle in this *Kras/Lkb1* lung cancer model, it blocked metastasis (Table S2).

Gene expression profiling of short term treated tumors showed that all treatments were able to revert Lkb1 and Mets signatures (Table S2). Interestingly, Dasatinib alone induced downregulation of SRC, TGF-β, and MEK signatures, but not AKT, EMT, and ES signatures. Triple combination downregulated SRC, TGF-β, MEK, as well as AKT, EMT, and ES signatures. This analysis supports the observation that Dasatinib synergizes with BEZ/AZD in inhibiting signal transduction pathways that are important in the proliferation and survival of *Kras/Lkb1*-driven cancer cells.

DISCUSSION

Cancer genomic studies have established a number of oncogene and tumor suppressor pathways as important for the initiation and maintenance of neoplastic lesions in NSCLC. However, the molecular alterations necessary for invasion and metastasis of NSCLC are less well-defined. We have previously reported that deletion of the *Lkb1* tumor suppressor gene in the context of *Kras*-driven murine lung tumors promotes invasion and metastasis (Ji et al., 2007). Here we extend these findings to show that *Kras/Lkb1* primary and metastatic tumors have upregulated expression of markers and inducers of EMT. Furthermore, through an integrated genomic and phosphoproteomic analysis of mouse lung primary and metastatic tumors, we have determined that two key modulators of focal adhesion dynamics, SRC and FAK, are upregulated by *Lkb1* loss during NSCLC progression. Similarly, LKB1 loss in vitro also resulted in SRC activation, increased motility, and SRC-dependent adhesion. In fact, migration was selectively abrogated by SRC and FAK inhibition in LKB1-deficient cells. Finally, whereas *Kras* mutant lung tumors are sensitive to the combined inhibition of the PI3K and MEK pathways, we have found that *Kras/Lkb1* tumors are resistant to these inhibitors, and that sensitivity can be restored by additional targeting of SRC. It also important to note that addition of Dasatinib to combined PI3K/MEK inhibition induced tumor shrinkage in the LKB1-deficient tumors. This reveals an important role for SFKs in tumor growth and promoting resistance to combined PI3K/MEK inhibition. Indeed, in addition to their prominent roles in tumor migration and adhesion, SFKs are also essential for transducing signals from RTKs and integrins to promote cell survival and proliferation (Yeatman, 2004). It was somewhat surprising that single-agent Dasatinib led to increased volume of *Kras/Lkb1* tumors (Figure 6) and persisting Akt and EMT signatures (Table S3). Although we cannot fully explain this observation, it is tempting to speculate that SRC inhibition led to loss of a feedback mechanism resulting in increased tumor growth or to a change in the interactions between tumor cells and stroma or immune cells resulting in tumor growth. Collectively, these results point toward a mechanism underlying the increased propensity for metastases seen in *Lkb1*-deficient lung tumors and identify SRC as a molecularly targetable pathway for the treatment of *LKB1*-deficient NSCLC in humans.

Tumor metastasis is a complex, multistage process that involves both initiating functions, such as invasion and angiogenesis, as well as metastasis progression functions such as extravasation and survival (Nguyen and Massague, 2007). EMT has been implicated in metastasis initiation and involves loss of cell-cell junction proteins as well as a conversion of stationary cells to motile cells capable of invading through the ECM (Yang and Weinberg, 2008). Our gene expression analysis suggests that LKB1 loss results in the aberrant expression of a number of oncogenic pathways and transcription factors known to be inducers of EMT such as *SNAI1, TWIST1,* and the TGF-β and β-catenin pathways (Kalluri and Weinberg, 2009; Nguyen and Massague, 2007; Yang and Weinberg, 2008). Although the mechanism by which LKB1 loss promotes EMT remains to be determined, we observe that NSCLC cells lacking LKB1 exhibit higher nuclear localization of β-catenin and increased release of TGF-β (Figures S3F and S3G) suggesting that LKB1 loss may have a direct cell autonomous role in promoting the EMT program. The expression signatures derived from *Kras/Lkb1* metastasis enriched for EMT correlate with NSCLC patients with metastatic potential and worsened survival (Figure 1B), whereas expression signatures derived from *Kras* primary tumors or *Kras/Lkb1* tumors did not correlate with survival thus have no prognostic value. Importantly, the presence of *Mets* signature in primary tumor samples, including a subset of double *KRAS* and *LKB1* mutants, suggests that a subset of primary tumors harbor cells destined for metastasis.

Part of the roadblock in defining the pathways involved in invasion and metastases in human NSCLC has been the difficulty in obtaining tissue from metastatic sites. Through the use of a *Kras*-driven, *Lkb1*-deficient genetically engineered mouse model of lung cancer, we have been able to collect matched primary and metastatic tumors and apply integrated gene expression and phosphoproteomic analysis to define altered signal transduction pathways. The utilization of complex murine cancer models to identify signal transduction pathways altered in cancer progression and metastases might serve as a paradigm for other solid tumors that suffer from similar barriers to tissue acquisition.

Previous work from our lab has shown that dual inhibition of the PI3K and MEK pathways in *Kras*-driven murine NSCLC results in synergistic tumor responses (Engelman et al., 2008). Strikingly, *Lkb1* loss renders these tumors substantially more resistant to this therapeutic regimen; therefore, *Lkb1* loss could serve as a negative predictor of the responses to the therapy. Despite the broad gene expression changes seen in the setting of *Lkb1* loss and progression to metastases, it is notable that we were able to define a candidate mediator of *Lkb1*-deficient tumor growth, SRC, in which additional inhibition—with Dasatinib—was able to restore sensitivity to inhibition of PI3K and MEK in vivo. A limitation of this analysis is that Dasatinib is a potent inhibitor of other kinases, e.g., ABL, which was also activated to a lesser degree in Lkb1-deficient tumors. Future studies will determine the relative importance of SFKs versus other Dasatinib targets in mediating the response to this agent. Lastly, *Kras/Lkb1* mice treated with Dasatinib alone did not show any evidence of metastasis (Table S2). This further reinforces our data that the Src family members are important mediators of metastatic progression in *Kras/Lkb1*-driven lung cancer. In conclusion, our results imply that despite the complex transcriptional and signaling changes that occur in the setting of LKB1 loss and progression of NSCLC, these tumors may still be addicted to isolated oncogenic events that can be successfully therapeutically targeted.

EXPERIMENTAL PROCEDURES

Mouse Colony and Tumor Collection

All mice were housed and treated in accordance with protocols approved by the institutional care and use committees for animal research at the Dana-Farber Cancer Institute. *Kras* and *Kras/Lkb1* mice were treated with 5×10^6 p.f.u. adeno-Cre (University of Iowa viral vector core) intranasally as previously described (Ji et al., 2007). Primary lung adenocarcinomas and metastases were macrodissected and formalin fixed or frozen in liquid nitrogen and stored at −80°C until use.

Histology and Immunohistochemical Analysis

Formalin-fixed tissues were paraffin embedded, sectioned at 5 μm, and hematoxylin and eosin (H&E) stained (Department of Pathology in Brigham and Women's Hospital). Unstained slides were deparaffinized in xylene and rehydrated sequentially in ethanol. Antigen retrieval was performed by boiling slides in 10 mM sodium citrate (pH 6.0) for 30 min. Primary antibodies were diluted in TBST with 5% goat serum and incubated overnight at 4°C (see Supplemental experimental procedures for detailed list of primary antibodies). Detection was performed using the avidin-biotin horseradish peroxidase technique in which 3,3′-diaminobenzidine was the chromogenic substrate.

Analysis of Microarray Gene Expression Data

Gene expression profiling methods (Total RNA isolation and microarray processing) are available in Supplemental Experimental Procedures. Clustering and differential expression analyses were performed using the Gepas Analysis suite (Tarraga et al., 2008) and GenePattern (Reich et al., 2006) with procedures described in Supplemental Experimental Procedures. Genomica software (http://genomica.weizmann.ac.il/) was used to identify enrichment patterns of a custom collection of experimental signatures associated with different phenotypes and cancer-related events (Ben-Porath et al., 2008; Segal et al., 2004) (see Table S1 for detailed description). In brief, the data were log2 transformed and mean centered. Genes whose expression was 2-fold or greater than the mean expression level were scored. Enrichment of overexpressed or underexpressed genes that belong to each tested gene signature was calculated using a hypergeometric test and an FDR calculation to account for multiple hypothesis testing. ($p < 0.05$, FDR < 0.05). Finally, the fraction of tumors showing significant enrichment for a particular gene signature in each class (*Kras* tumors, *Kras/Lkb1* primary tumors and metastasis) was calculated and assigned a p value according to the hypergeometric distribution ($p < 0.01$, FDR < 0.05).

Gene Set Enrichment analysis of short-term treated *Kras/Lkb1* tumors was performed using GSEA (http://broad.mit.edu/gsea) across the complete list of genes ranked by signal-to-noise ratio.

UNC human lung cancer microarrays (Agilent custom 44,000 probe) annotated with *KRAS* and *LKB1* genetic status were mapped to mouse genes using NCBI Homologene, retaining only one-to-one orthologs. Microarray data were sample and gene standardized, and Lkb1 and Mets signature scores were calculated as the median of the genes across the gene set. Statistical significance was calculated using the Wilcoxon rank sum test.

Survival Analysis

The Director's Challenge Consortium human primary lung adenocarcinoma data set was downloaded from http://caarraydb.nci.nih.gov (experiment ID 1015945236141280:1) (Shedden et al., 2008). MSKK data set 2 was downloaded from http://cbio.mskcc.org/Public/lung_array_data (Nguyen et al., 2009). Data sets were first log2 transformed, mean-centered data set and loaded into Genomica software. Enrichment of genes that belong to our murine-derived Mets signature was calculated as described above and each patient was assigned an enrichment score. Positive and negative enrichment scores for each individual were matched with survival data (time to last contact or death) or recurrence of metastasis (metastasis-free survival). Kaplan-Meier plots were created with Graphpad software. Statistical significance was calculated using the log-rank test.

Phosphopeptide Immunoprecipitation, Liquid-Chromatography Tandem MS, and Phosphopeptide Analysis

We performed phosphotyrosine peptide identification and quantification as described previously (Rikova et al., 2007). See Supplemental Experimental Procedures for sample preparation and handling. For differential phosphorylation analysis, duplicated intensities were averaged, and fold-changes between different experimental conditions were calculated. For KEGG classification of the phosphoproteins, we used FatiGO software (www.babelomics.org) (Al-Shahrour et al., 2004). A modification of GSEA (Subramanian et al., 2005) with phosphoprotein sets instead gene sets (Figure S2A) was used to interrogate the PhosphoPoint database of tyrosine kinase substrates (http://kinase.bioinformatics.tw) (Yang et al., 2008).

Quantitative RT-PCR

A total of 50 ng RNA total RNA was reverse transcribed with the Superscript cDNA Synthesis Kit (Invitrogen). RT-PCR reactions were prepared in triplicate for each sample using primers and TaqMan probes purchased from Applied Biosystems (see also Supplemental Experimental Procedures). Reactions were run on an ABI PRISM 7900HT Sequence Detection System (Applied Biosystems). GAPDH was used as a reference for all reactions. Relative levels of a gene were determined by ΔΔCt method.

Multiplex Bead Analysis

Quantification of TGF-β isoforms and Src family kinase activities were assayed using Human TGF-β 1,2,3 Assay and SRC Family Kinase 8-Plex (Millipore), respectively. Assays were performed according to the manufacturer's specifications and analyzed with a Luminex 100 platform. Fluorescence intensity from duplicate samples was averaged and transformed into protein concentration using a calibration curve obtained with TGFβ1, 2, and 3 standards. For Src assay, activity was expressed in mean fluorescence intensity with background correction from duplicate samples. Statistical significance was calculated using a two-sided Student's exact t test.

Western Blot and Kinase Array Analysis

Parameters for western blot and antibodies are available in Supplemental Experimental Procedures. Human phosphokinase arrays (R&D Systems) were performed according to the manufacturer's instructions. The percent control activation/deactivation was determined by densitometric analysis using ImageJ Software (NIH).

Short Hairpin RNA Constructs, Lentiviral Infection, and Small Interfering RNA Infection

Short hairpin RNA (shRNA) constructs cloned in pLKO.1 puro vector were designed by the RNAi consortium and distributed by Open Biosystems. shRNA sequences are provided with supplemental experimental procedures. Stable polyclonal cell lines are established as described previously (Shimamura et al., 2008).

Cell Migration, Invasion, and Adhesion Assays

Cell migration in cultures was measured using a two-dimensional in vitro scratch motility assay. A 1 mm wide scratch was made on confluent monolayer in tissue culture slides and allowed to grow under standard conditions for 12 hr. Repopulation of the cleared field was recorded using a Nikon inverted TE2000 and migrated distance was quantified using Image J software. Invasion and adhesion assays kits were obtained from Cell Biolabs and assays were performed according to the manufacturer's specifications. Details are available in the Supplemental Experimental Procedures.

Immunofluorescence Analysis

Cells were fixed on four-well chamber glass slides in methanol/acetone (1:1) at –20°C for 10 min and air dried. Primary block was done with 10% goat serum (Sigma) and 0.05% Tween 20 in phosphate-buffered saline for 1 hr at room temperature. A mouse monoclonal antibody for activated β-catenin (Millipore) was diluted 1:50 in blocking buffer and incubated overnight at 4°C. Rabbit anti-mouse secondary antibody conjugated with Alexa488 dye (Invitrogen) was diluted 1:100 in blocking buffer and incubated for 1 hr at room temperature. Images were acquired using a Nikon inverted TE2000 microscope equipped a Hamamatsu Orca ER digital CCD camera.

In Vivo Xenograft Experiments

The 5- to 6-week-old female nu/nu mice (Charles River) were maintained under pathogen-free conditions. Tumors were generated by injecting subcutaneous 5×10^6 cells mixed with reconstituted basement membrane Matrigel (BD Biosciences) with 1:1 ratio in PBS. Animals were sacrificed 14 days after inoculation, and tumors were excised and fixed in formalin. Tumor measurements were obtained using electronic calipers. Tumor volume was calculated using: Tumor volume = (length × width^2)/2. We compared tumor volumes of mice using a two-sided Student's exact t test.

Cancer Therapy with Inhibitors

Dual PI3K-mTOR inhibitor, NVP-BEZ235-AN (Novartis Institutes for Biomedical Research) was reconstituted in one volume of *N*-methyl-2-pyrrolidone (69118, Fluka) and nine volumes of PEG300 (81160, Fluka) and administered by oral gavage. MEK inhibitor ARRY-142886 (AZD6244, Otava Chemicals) and Dasatinib (LC Labs) were reconstituted in 0.5% methyl cellulose (Fluka) and 0.4% polysorbate (Tween 80; Fluka) and administered by oral gavage. Dosages are indicated in the figure legends.

MRI and Tumor Volume Measurement

We performed MRI measurements as described previously (Engelman et al., 2008). Brief descriptions are available in the Supplemental Experimental Procedures.

ACCESSION NUMBERS

Microarray data have been deposited at GEO with the accession number GSE21581.

SUPPLEMENTAL INFORMATION

Supplemental Information includes three figures, three tables, and Supplemental Experimental Procedures and can be found with this article online at doi:10.1016/j.ccr.2010.04.026.

ACKNOWLEDGMENTS

J.C. was a fellow of Spanish Ministry of Science and Innovation (MICINN) and Spanish Association against Cancer (AECC). T.S. was supported by the DF/HCC Claudia Adams Barr Program in Innovative Basic Cancer Research. K.-K.W. and J.A.E. are founders of Gatekeeper Therapeutics. This work was supported by Dana-Farber-Harvard Cancer Center Lung Cancer Specialized Program of Research Excellence (SPORE) grant P50 CA090578 (J.A.E. and K.-K.W.); U01CA141576 (K.-K.W., D.C., N.S. and N.B.) R01 AG2400401 (K.-K.W.), R01 CA122794 (K.-K.W.), R01 CA140594 (J.A.E. and K.-K.W.), 1RC2CA147940-01 (J.A.E. and K.-K.W.), K08 grant CA120060 (J.A.E.), R01CA137008 (J.A.E.), DF/HCC Gastrointestinal Cancer SPORE P50 CA127003 (J.A.E.); American Association for Cancer Research (J.A.E.); V Foundation (J.A.E.); American Cancer Society RSG-06-102-01-CCE (J.A.E.); and Ellison Foundation Scholar (J.A.E.). K.R., K.C., J.C.S. and T.-L.G. are employees of Cell Signaling Technology. C.G.-E. and S.-M.M. are employees of Novartis Institutes for Biochemical Research. J.A.E. receives research funding from Novartis. We thank H. Voelker for help in preparation of this manuscript.

Received: November 3, 2009
Revised: March 12, 2010
Accepted: May 7, 2010
Published: June 14, 2010

REFERENCES

Al-Shahrour, F., Diaz-Uriarte, R., and Dopazo, J. (2004). FatiGO: A web tool for finding significant associations of Gene Ontology terms with groups of genes. Bioinformatics *20*, 578–580.

Alessi, D.R., Sakamoto, K., and Bayascas, J.R. (2006). LKB1-dependent signaling pathways. Annu. Rev. Biochem. *75*, 137–163.

Arthur, W.T., Petch, L.A., and Burridge, K. (2000). Integrin engagement suppresses RhoA activity via a c-Src-dependent mechanism. Curr. Biol. *10*, 719–722.

Ben-Porath, I., Thomson, M.W., Carey, V.J., Ge, R., Bell, G.W., Regev, A., and Weinberg, R.A. (2008). An embryonic stem cell-like gene expression signature in poorly differentiated aggressive human tumors. Nat. Genet. *40*, 499–507.

Bild, A.H., Yao, G., Chang, J.T., Wang, Q., Potti, A., Chasse, D., Joshi, M.B., Harpole, D., Lancaster, J.M., Berchuck, A., et al. (2006). Oncogenic pathway signatures in human cancers as a guide to targeted therapies. Nature *439*, 353–357.

Burridge, K., Chrzanowska-Wodnicka, M., and Zhong, C. (1997). Focal adhesion assembly. Trends Cell Biol. *7*, 342–347.

Carretero, J., Medina, P.P., Blanco, R., Smit, L., Tang, M., Roncador, G., Maestre, L., Conde, E., Lopez-Rios, F., Clevers, H.C., and Sanchez-Cespedes, M. (2007). Dysfunctional AMPK activity, signalling through mTOR and survival in response to energetic stress in LKB1-deficient lung cancer. Oncogene *26*, 1616–1625.

Carretero, J., Medina, P.P., Pio, R., Montuenga, L.M., and Sanchez-Cespedes, M. (2004). Novel and natural knockout lung cancer cell lines for the LKB1/STK11 tumor suppressor gene. Oncogene *23*, 4037–4040.

Cole, M.F., Johnstone, S.E., Newman, J.J., Kagey, M.H., and Young, R.A. (2008). Tcf3 is an integral component of the core regulatory circuitry of embryonic stem cells. Genes Dev. *22*, 746–755.

Engelman, J.A., Chen, L., Tan, X., Crosby, K., Guimaraes, A.R., Upadhyay, R., Maira, M., McNamara, K., Perera, S.A., Song, Y., et al. (2008). Effective use of PI3K and MEK inhibitors to treat mutant Kras G12D and PIK3CA H1047R murine lung cancers. Nat. Med. *14*, 1351–1356.

Hearle, N., Schumacher, V., Menko, F.H., Olschwang, S., Boardman, L.A., Gille, J.J., Keller, J.J., Westerman, A.M., Scott, R.J., Lim, W., et al. (2006). Frequency and spectrum of cancers in the Peutz-Jeghers syndrome. Clin. Cancer Res. *12*, 3209–3215.

Huveneers, S., and Danen, E.H. (2009). Adhesion signaling -crosstalk between integrins, Src and Rho. J. Cell Sci. *122*, 1059–1069.

Iwanaga, K., Yang, Y., Raso, M.G., Ma, L., Hanna, A.E., Thilaganathan, N., Moghaddam, S., Evans, C.M., Li, H., Cai, W.W., et al. (2008). Pten inactivation accelerates oncogenic K-ras-initiated tumorigenesis in a mouse model of lung cancer. Cancer Res. *68*, 1119–1127.

Jackson, E.L., Olive, K.P., Tuveson, D.A., Bronson, R., Crowley, D., Brown, M., and Jacks, T. (2005). The differential effects of mutant p53 alleles on advanced murine lung cancer. Cancer Res. *65*, 10280–10288.

Jackson, E.L., Willis, N., Mercer, K., Bronson, R.T., Crowley, D., Montoya, R., Jacks, T., and Tuveson, D.A. (2001). Analysis of lung tumor initiation and progression using conditional expression of oncogenic K-ras. Genes Dev. *15*, 3243–3248.

Ji, H., Li, D., Chen, L., Shimamura, T., Kobayashi, S., McNamara, K., Mahmood, U., Mitchell, A., Sun, Y., Al-Hashem, R., et al. (2006a). The impact of human EGFR kinase domain mutations on lung tumorigenesis and in vivo sensitivity to EGFR-targeted therapies. Cancer Cell *9*, 485–495.

Ji, H., Ramsey, M.R., Hayes, D.N., Fan, C., McNamara, K., Kozlowski, P., Torrice, C., Wu, M.C., Shimamura, T., Perera, S.A., et al. (2007). LKB1 modulates lung cancer differentiation and metastasis. Nature *448*, 807–810.

Ji, H., Zhao, X., Yuza, Y., Shimamura, T., Li, D., Protopopov, A., Jung, B.L., McNamara, K., Xia, H., Glatt, K.A., et al. (2006b). Epidermal growth factor receptor variant III mutations in lung tumorigenesis and sensitivity to tyrosine kinase inhibitors. Proc. Natl. Acad. Sci. USA *103*, 7817–7822.

Johnson, F.M., Saigal, B., Talpaz, M., and Donato, N.J. (2005). Dasatinib (BMS-354825) tyrosine kinase inhibitor suppresses invasion and induces cell cycle arrest and apoptosis of head and neck squamous cell carcinoma and non-small cell lung cancer cells. Clin. Cancer Res. *11*, 6924–6932.

Kalluri, R., and Weinberg, R.A. (2009). The basics of epithelial-mesenchymal transition. J. Clin. Invest. *119*, 1420–1428.

Kim, W., Perera, S., Zhou, B., Carretero, J., Yeh, J., Heathcote, S., Jackson, A., Nikolinakos, P., Ospina, B., Naumov, G., et al. (2009). HIF2α cooperates with RAS to promote lung tumorigenesis in mice. J. Clin. Invest. *119*, 2160–2170.

Koivunen, J.P., Kim, J., Lee, J., Rogers, A.M., Park, J.O., Zhao, X., Naoki, K., Okamoto, I., Nakagawa, K., Yeap, B.Y., et al. (2008). Mutations in the LKB1 tumour suppressor are frequently detected in tumours from Caucasian but not Asian lung cancer patients. Br. J. Cancer *99*, 245–252.

Matsumoto, S., Iwakawa, R., Takahashi, K., Kohno, T., Nakanishi, Y., Matsuno, Y., Suzuki, K., Nakamoto, M., Shimizu, E., Minna, J.D., and Yokota, J. (2007). Prevalence and specificity of LKB1 genetic alterations in lung cancers. Oncogene *26*, 5911–5918.

Mitra, S.K., and Schlaepfer, D.D. (2006). Integrin-regulated FAK-Src signaling in normal and cancer cells. Curr. Opin. Cell Biol. *18*, 516–523.

Nevins, J.R., and Potti, A. (2007). Mining gene expression profiles: Expression signatures as cancer phenotypes. Nat. Rev. Genet. *8*, 601–609.

Nguyen, D.X., Chiang, A.C., Zhang, X.H., Kim, J.Y., Kris, M.G., Ladanyi, M., Gerald, W.L., and Massague, J. (2009). WNT/TCF signaling through LEF1 and HOXB9 mediates lung adenocarcinoma metastasis. Cell *138*, 51–62.

Nguyen, D.X., and Massague, J. (2007). Genetic determinants of cancer metastasis. Nat. Rev. Genet. *8*, 341–352.

Onder, T.T., Gupta, P.B., Mani, S.A., Yang, J., Lander, E.S., and Weinberg, R.A. (2008). Loss of E-cadherin promotes metastasis via multiple downstream transcriptional pathways. Cancer Res. *68*, 3645–3654.

Playford, M.P., and Schaller, M.D. (2004). The interplay between Src and integrins in normal and tumor biology. Oncogene *23*, 7928–7946.

Reddel, R.R., Ke, Y., Kaighn, M.E., Malan-Shibley, L., Lechner, J.F., Rhim, J.S., and Harris, C.C. (1988). Human bronchial epithelial cells neoplastically transformed by v-Ki-ras: altered response to inducers of terminal squamous differentiation. Oncogene Res. *3*, 401–408.

Reich, M., Liefeld, T., Gould, J., Lerner, J., Tamayo, P., and Mesirov, J.P. (2006). GenePattern 2.0. Nat. Genet. *38*, 500–501.

Rikova, K., Guo, A., Zeng, Q., Possemato, A., Yu, J., Haack, H., Nardone, J., Lee, K., Reeves, C., Li, Y., et al. (2007). Global survey of phosphotyrosine signaling identifies oncogenic kinases in lung cancer. Cell *131*, 1190–1203.

Sanchez-Cespedes, M., Parrella, P., Esteller, M., Nomoto, S., Trink, B., Engles, J.M., Westra, W.H., Herman, J.G., and Sidransky, D. (2002). Inactivation of LKB1/STK11 is a common event in adenocarcinomas of the lung. Cancer Res. *62*, 3659–3662.

Segal, E., Friedman, N., Koller, D., and Regev, A. (2004). A module map showing conditional activity of expression modules in cancer. Nat. Genet. *36*, 1090–1098.

Shaw, R.J., Bardeesy, N., Manning, B.D., Lopez, L., Kosmatka, M., DePinho, R.A., and Cantley, L.C. (2004). The LKB1 tumor suppressor negatively regulates mTOR signaling. Cancer Cell *6*, 91–99.

Shedden, K., Taylor, J.M., Enkemann, S.A., Tsao, M.S., Yeatman, T.J., Gerald, W.L., Eschrich, S., Jurisica, I., Giordano, T.J., Misek, D.E., et al. (2008). Gene expression-based survival prediction in lung adenocarcinoma: A multi-site, blinded validation study. Nat. Med. *14*, 822–827.

Shibue, T., and Weinberg, R.A. (2009). Integrin beta1-focal adhesion kinase signaling directs the proliferation of metastatic cancer cells disseminated in the lungs. Proc. Natl. Acad. Sci. USA *106*, 10290–10295.

Shimamura, T., Li, D., Ji, H., Haringsma, H.J., Liniker, E., Borgman, C.L., Lowell, A.M., Minami, Y., McNamara, K., Perera, S.A., et al. (2008). Hsp90 inhibition suppresses mutant EGFR-T790M signaling and overcomes kinase inhibitor resistance. Cancer Res. *68*, 5827–5838.

Slack-Davis, J.K., Martin, K.H., Tilghman, R.W., Iwanicki, M., Ung, E.J., Autry, C., Luzzio, M.J., Cooper, B., Kath, J.C., Roberts, W.G., and Parsons, J.T. (2007). Cellular characterization of a novel focal adhesion kinase inhibitor. J. Biol. Chem. *282*, 14845–14852.

Subramanian, A., Tamayo, P., Mootha, V.K., Mukherjee, S., Ebert, B.L., Gillette, M.A., Paulovich, A., Pomeroy, S.L., Golub, T.R., Lander, E.S., and Mesirov, J.P. (2005). Gene set enrichment analysis: a knowledge-based approach for interpreting genome-wide expression profiles. Proc. Natl. Acad. Sci. USA *102*, 15545–15550.

Tarraga, J., Medina, I., Carbonell, J., Huerta-Cepas, J., Minguez, P., Alloza, E., Al-Shahrour, F., Vegas-Azcarate, S., Goetz, S., Escobar, P., et al. (2008). GEPAS, a web-based tool for microarray data analysis and interpretation. Nucleic Acids Res. *36*, W308–W314.

Thomson, S., Petti, F., Sujka-Kwok, I., Epstein, D., and Haley, J.D. (2008). Kinase switching in mesenchymal-like non-small cell lung cancer lines contributes to EGFR inhibitor resistance through pathway redundancy. Clin. Exp. Metastasis *25*, 843–854.

Yang, C.Y., Chang, C.H., Yu, Y.L., Lin, T.C., Lee, S.A., Yen, C.C., Yang, J.M., Lai, J.M., Hong, Y.R., Tseng, T.L., et al. (2008). PhosphoPOINT: a comprehensive human kinase interactome and phospho-protein database. Bioinformatics *24*, i14–i20.

Yang, J., and Weinberg, R.A. (2008). Epithelial-mesenchymal transition: at the crossroads of development and tumor metastasis. Dev. Cell *14*, 818–829.

Yeatman, T.J. (2004). A renaissance for SRC. Nat. Rev. Cancer *4*, 470–480.